nanomaterials

MDPI

Article

Effect of Serum Albumin on Porphyrin-Quantum Dot Complex Formation, Characteristics and Spectroscopic Analysis

André L. S. Pavanelli [1], Leandro N. C. Máximo [2], Roberto S. da Silva [3] and Iouri E. Borissevitch [1,*]

[1] Departamento de Física, Faculdade de Filosofia, Ciências e Letras de Ribeirão Preto, Universidade de São Paulo, Av. Bandeirantes 3900, Ribeirão Preto 14040-900, Brazil; andpavanelli@gmail.com
[2] Instituto Federal de Educação, Ciência e Tecnologia Goiano, Urutaí 75790-000, Brazil; lncmaximo@gmail.com
[3] Departamento de Ciências Biomoleculares, Faculdade de Ciências Farmacêuticas de Ribeirão Preto, Universidade de São Paulo, Av. Bandeirantes 3900, Ribeirão Preto 14040-900, Brazil; silva@usp.br
* Correspondence: iourib@ffclrp.usp.br; Tel.: +55-16-3315-3862; Fax: +55-16-3315-4887

Abstract: The effect of bovine serum albumin (BSA) upon interaction between CdTe QD functionalized by 3-Mercaptopropionic Acid (CdTe-3-MPA QD) and two water soluble porphyrins: positively charged *meso*-tetra methyl pyridyl porphyrin (TMPyP) and negatively charged *meso*-tetrakis(p-sulfonato-phenyl) porphyrin ($TPPS_4$), was studied in function of pH using the steady-state and time resolved optical absorption and fluorescence spectroscopies. It was shown that, depending on the charge state of the components, interaction with albumin could either prevent the formation of the QD ... PPh complex, form a mixed QD ... PPh ... BSA complex or not affect PPh complexation with QD at all. The obtained results may be of interest for application in photomedicine.

Keywords: CdTe-3-MPA quantum dot; $TPPS_4$ and TMPyP porphyrins; quantum dot-porphyrin complex; bovine serum albumin effects; pH effect

Citation: Pavanelli, A.L.S.; Máximo, L.N.C.; da Silva, R.S.; Borissevitch, I.E. Effect of Serum Albumin on Porphyrin-Quantum Dot Complex Formation and Characteristics. Spectroscopic Analysis. *Nanomaterials* **2021**, *11*, 1674. https://doi.org/10.3390/nano11071674

Academic Editor: Miryana Hemadi

Received: 7 May 2021
Accepted: 21 June 2021
Published: 25 June 2021

1. Introduction

Photodynamic therapy (PDT) is a method of treatment of various diseases, including several types of cancer [1–6]. PDT is based on mutual application of a photoactive compound (photosensitizer, PS), visible or infrared light and molecular oxygen to generate reactive oxygen species (ROS). The efficacy of PDT depends on the PS structural characteristics, which are important to increase its uptake and subcellular localization. Porphyrin-type compounds are of a special interest among PS. Due to their intensive optical absorption in the required spectral regions, high quantum yield of the triplet state and relative intense fluorescence, high dark and photostability and affinity with biological structures, such as proteins, nucleic acids and cell membranes, porphyrins (PPh) are widely applied as PS in Photodynamic Therapy (PDT) [1–6] and as fluorescence probes in Fluorescence Diagnostics (FD) [7,8]. However, a great disadvantage of PPh for these applications lies in their relatively low optical absorption in the spectral region of the so-called phototherapeutic window (600–800 nm), where biological tissues are the most transparent. The problem could be corrected by PPh complexation with certain structures, able to absorb light energy in this spectral range and transfer this energy to PPh molecules.

Semiconductor nanocrystals (quantum dots, QD) possess intense optical absorption in a wide spectral range and intensive and narrow fluorescence band, the position of which depends on QD core size [9]. Due to these extraordinary characteristics, QD can serve as an antenna, accumulating the light energy in a wide spectral region and passing it to other compounds, PPh, in particular [10–13].

On the other hand, being inorganic semiconductors, QDs manifest high toxicity toward biological objects and possess low water solubility, which restricts their direct application in medicine and biology. However, when the QD surface is covered with appropriate molecules (functionalized QD), it overcomes this imperfection, as in this case

living systems appear protected from the contact with the toxic QD core (CdTe or CdSe, for example). Moreover, functionalization of the QD surface by specific groups, for example, aptamers, can increase their affinity to specific biological targets, malignant tissues in particular [14,15]. This makes QD a promising drug delivery system [16–18].

At the same time, the mechanisms of QD action in photochemotherapy, not well studied yet, differ from the photodynamic effect, the basis of the photodynamic therapy (PDT), which is effective and well described. Therefore, the complexes of porphyrins with quantum dots are of great interest for medicine. PPh and QD complexation can occur via energy, electron or proton transfer, depending on the structural characteristics of the participants [19–29].

When introduced into an organism, PPh and QD should interact with various organized structures, such as cell membranes, nucleic acids, proteins, etc. Among them, serum albumin attracts a special attention due to its ability to bind various compounds and transport them within the organism with blood flux [30]. Besides, albumins possess elevated affinity to malignant tissues [31,32]. This makes albumins perspective compounds as delivery systems. On the other hand, interaction with albumins can affect complexation of PPh with QD, changing its and the complex characteristics.

In the present work, we have studied the effect of bovine serum albumin on interaction between CdTe QD functionalized by 3-mercaptopropionic acid (CdTe-3-MPA QD) and two water soluble porphyrins: positively charged *meso*-tetra methyl pyridyl porphyrin (TMPyP) and negatively charged *meso*-tetrakis(p-sulfonato-phenyl) porphyrin ($TPPS_4$). The study was realized at pH 7.0 and pH 4.0 using optical absorption and fluorescence spectroscopies. It was shown that, depending on the charge state of components, interaction with albumin could produce various effects: prevent formation of the QD . . . PPh complex, form a mixed QD . . . PPh . . . BSA complex or not affect the PPh complexation with QD at all. The obtained results may be of interest for application in photomedicine.

2. Materials and Methods

TMPyP and $TPPS_4$ porphyrins (Figure 1) were purchased from Mid Century Chemicals (Posen, IL, USA), and used without any additional purification. Bovine serum albumin (BSA) was obtained from Sigma Aldrich Products (San Luis, MO, USA). CdTe-3-MPA QD were synthesized at the Department of Biomolecular Sciences of the Faculty of Pharmaceutic Sciences, Sao Paulo University, Brazil. The synthesis was realized in an aqueous media from Cd^{2+} and Te^{2-} solutions in accordance with the procedure described in details in [33] with some modifications. The solution was prepared by adding the oxygen-free NaHTe solution to the Cd^{2+} precursor solution at pH 11, in the absence of light, under continuous argon flow.

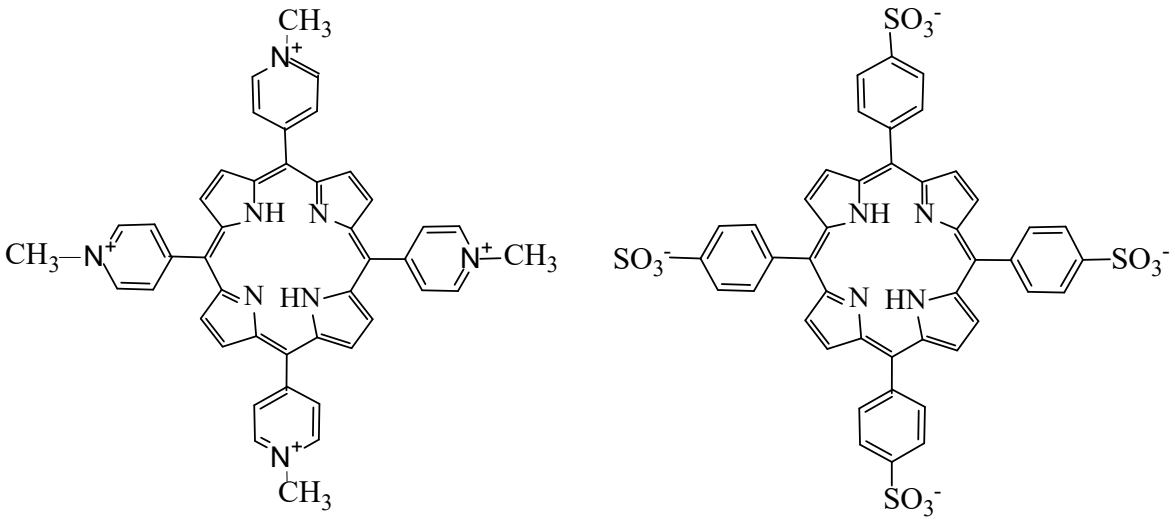

Figure 1. Chemical structures of TMPyP (**left**) and $TPPS_4$ (**right**).

The QD diameter (D) and molar absorption coefficient (ε), were calculated by the Equations (1) and (2) [34]:

$$D = \left(9.8127 \times 10^{-7}\right)\lambda^3 - \left(1.7147 \times 10^{-3}\right)\lambda^2 + (1.0064)\lambda - 194.84 \quad (1)$$

$$\varepsilon = 10043\ (D)^{2.12} \quad (2)$$

leading to $D \approx 2.5$ nm and $\varepsilon_{\lambda 557\ nm} = 7.0 \times 10^5\ M^{-1}\ cm^{-1}$, respectively.

The compound concentrations were determined from optical absorption (A) as

$$C = \frac{A}{\varepsilon} \quad (3)$$

using molar absorption coefficients: for BSA $\varepsilon = 4.55 \times 10^4\ M^{-1}\ cm^{-1}$ at $\lambda = 280$ nm, for CdTe-3-MPA QD $\varepsilon = 1.27 \times 10^5\ M^{-1}\ cm^{-1}$ at $\lambda = 557$ nm, for TMPyP $\varepsilon = 2.26 \times 10^5\ M^{-1}\ cm^{-1}$ at $\lambda = 425$ nm, for non-protonated $TPPS_4$ form (pH 7.0) $\varepsilon = 1.3 \times 10^4\ M^{-1}\ cm^{-1}$ at $\lambda = 515$ nm and $\varepsilon = 3.26 \times 10^4\ M^{-1}\ cm^{-1}$ at $\lambda = 644$ nm for its biprotonated form (pH 4.0).

2.1. Steady-State Optical Absorption and Fluorescence Measurements

The absorption spectra were obtained with the help of a Beckman Coulter DU-640 spectrophotometer and the fluorescence spectra were monitored by a Hitachi 7000 spectrometer.

To exclude the effect of changes in optical absorption at excitation wavelengths, the fluorescence intensities obtained experimentally were corrected in accordance with the equation:

$$I_{corr} = \frac{I_{exp}}{A_{ex}} \quad (4)$$

where I_{exp} and I_{corr} are experimental and corrected fluorescence intensities, respectively, and A_{ex} is the absorbance at the excitation wavelength.

2.2. Measurements of Time Resolved Fluorescence

Time-resolved fluorescence experiments were made using the time-correlated single photon counting technique. The excitation source was a pulse titanium-sapphire laser Tsunami 3950 pumped by a Millena Xs laser, both from Spectra Physics, with 5 ps pulse width at the half height and 8.0 MHz frequency, controlled by the pulse picker 3980 from Spectra Physics. The excitation wavelengths were obtained by the BBO (GWN-23PL from Spectra Physics) crystal. The measurements were made with a FL9000 spectrometer from Edinburgh, adjusted in an 'L' configuration with the excitation source. The wavelengths for measurement were selected by a monochromator and the detection was made by a Hamamatsu R3809U photomultiplier. The average time response of the instrument was 100 ps.

The PPh, QD and BSA stock solutions were prepared in phosphate buffer (pH 6.8, 7.5 mM). All experiments were realized at room temperature (24 ± 1) °C.

The experimental data were treated using OriginPro 8 commercial program. All final values were average of three independent experiments.

3. Results and Discussion

The CdTe-3-MPA QD possess optical absorption in the spectral range from 200 nm to 650 nm with an accentuated peak in the range from 425 nm to 575 nm with $\lambda_{max} = 490$ nm (Figure 2A). The fluorescence emission spectra of the synthesized CdTe-3-MPA QD were measured with excitation at 490 nm. Figure 2B shows the emission spectra with a band in the region of 500 nm to 700 nm ($\lambda_{max} = 585$ nm).

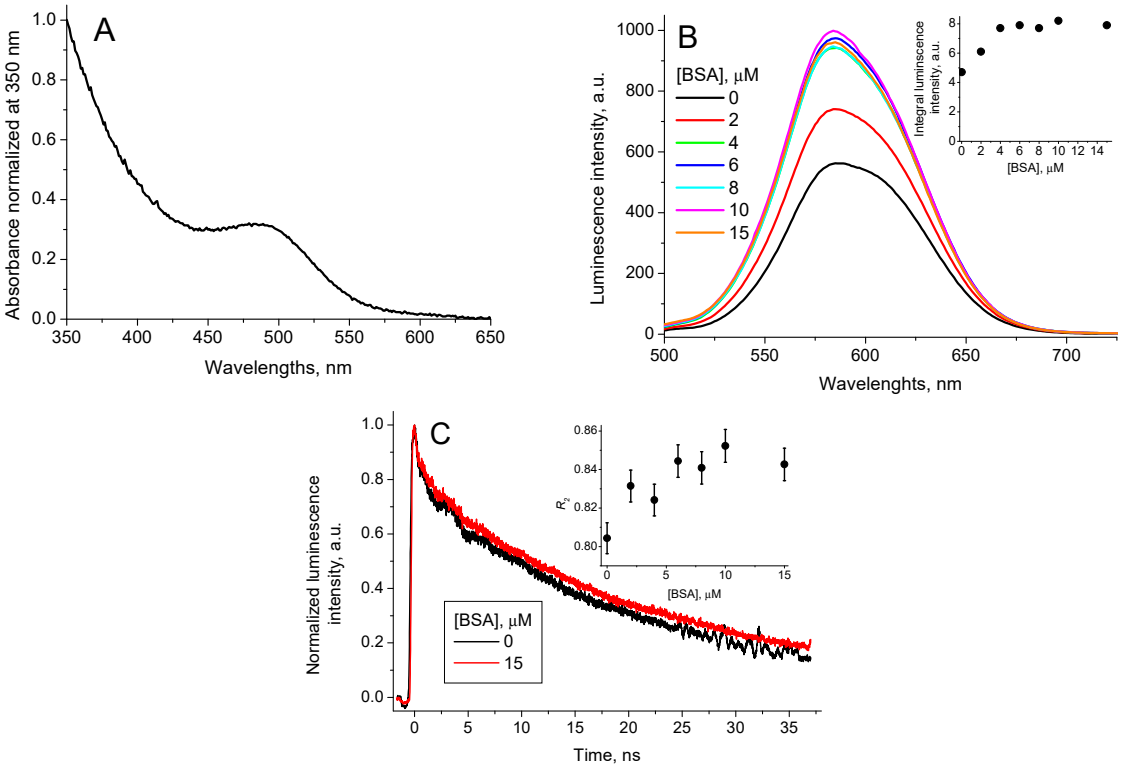

Figure 2. CdTe-3-MPA QD (**A**) absorption spectrum, normalized by absorbance at 350 nm, (**B**) QD luminescence spectrum (λ_{ex} = 490 nm) for different BSA concentrations, (inset: the integral QD luminescence intensity in function of the BSA concentration) and (**C**) QD luminescence decay curves (λ_{ex} = 490 nm, λ_{em} = 580 nm) for [BSA] = 0 and [BSA] = 15 μM (inset: the contribution of the long-lived luminescence decay component R_2 in function of the BSA concentration).

3.1. Quantum Dot Interaction with BSA

The results presented in this section were obtained at pH 7.0. At pH 4.0 we have observed no significant effect of BSA on QD characteristics in the concentration range used.

In an aqueous solution, BSA possesses UV-visible spectrum with maximum absorption at 280 nm and the fluorescence emission spectrum with maximum at 380 nm when excited at 280 nm. Interaction of BSA with CdTe-3-MPA QD in aqueous solutions show significant increase of the QD stability with no precipitation even after 24 h. The QD luminescence decay curves, registered for 480 nm excitation have been fitted successfully as the sum of two exponents (Figure 2C):

$$I = I_1 \times \exp(-t/\tau_{1QD\_BSA}) + I_2 \times \exp(-t/\tau_{2QD\_BSA}) \quad (5)$$

With lifetimes of the components τ_{1QD_BSA} = (0.9 ± 0.1) ns and τ_{2QD_BSA} = (20 ± 1) ns.

Addition of BSA does not affect the QD absorption spectrum, however, it increases the QD luminescence intensity (Figure 2B, inset). The profile of the QD luminescence decay curve continues biexponentially with invariable lifetimes of the components, and their relative amplitudes vary with the BSA concentration (Table 1).

The contribution of the respective component can be calculated as the ratio between its amplitude (I_1 or I_2) and the sum of amplitudes of both components ($I_1 + I_2$). Therefore, the contribution of the long-lived component, calculated as

$$R_2 = \frac{I_2}{I_1 + I_2} \quad (6)$$

where I_1 and I_2 are the amplitudes of the short-lived and the long-lived components, respectively, and suffer an increase, which coincides with the increase in the integral luminescence intensity (compare the insets on Figure 2B,C).

Table 1. Lifetimes of the short-lived (τ_1) and long-lived (τ_2) components of CdTe-3-MPA QD luminescence decay curves and their relative amplitudes (I_1, I_2) for different BSA concentrations.

[BSA], μM	τ_1, ns	I_1	τ_2, ns	I_2
0	0.913 ± 0.004	0.196 ± 0.002	20.5 ± 0.02	0.804 ± 0.008
2	0.867 ± 0.004	0.169 ± 0.002	21.4 ± 0.02	0.831 ± 0.008
4	0.920 ± 0.003	0.176 ± 0.002	19.6 ± 0.01	0.824 ± 0.008
6	0.903 ± 0.004	0.156 ± 0.002	18.9 ± 0.03	0.844 ± 0.008
8	0.867 ± 0.005	0.160 ± 0.002	18.0 ± 0.03	0.841 ± 0.008
10	0.888 ± 0.005	0.148 ± 0.002	21.5 ± 0.04	0.852 ± 0.008
15	0.922 ± 0.003	0.157 ± 0.002	20.4 ± 0.03	0.843 ± 0.008

Thus, it is possible to conclude that the increase of the QD luminescence intensity may be associated with increase of the contribution of the long-lived component R_2. Consequently, the contribution of the short-lived component decreases.

As it has been shown recently [13,26–29], the short-lived component of the CdTe-3-MPA QD luminescence is associated with the electron-hole annihilation in the QD core, while the long-lived one is due to the electron-hole annihilation in the QD functionalizing (protective) shell. Therefore, the increase of the QD luminescence intensity in the presence of BSA can be due to interaction of BSA with 3-MPA groups on the QD surface.

The binding constant of QD with BSA ($K_{\mathrm{QD\_BSA}}$) was calculated using the equation from [35]:

$$\frac{1}{I - I_{min}} = \frac{1}{I_{max} - I_{min}} + \frac{1}{(I_{max} - I_{min})K_{\mathrm{QD\_BSA}}} \frac{1}{[BSA]} \quad (7)$$

where I_{min}, I and I_{max} are integral luminescence intensities in the absence of BSA, for BSA concentration [BSA] and for the BSA excess.

The determined value was $K_{\mathrm{QD\_BSA}} = (1.2 \pm 0.1) \times 10^6\ \mathrm{M}^{-1}$.

The fact that at pH 4.0 no changes in the QD and BSA characteristics at used concentrations were observed may be explained by strong electrostatic repulsion between positively charged QD and BSA. Indeed, the isoelectric point (IP) of BSA is at pH 4.7 [30]. At the same time the $\mathrm{pK_a}$ point of CdTe-3-MPA QD is at pH 4.34 [36]. Thus, at pH 4.0 the total charge of both BSA and QD is positive, which should reduce the probability of their binding making the binding constant much less than $(1.2 \pm 0.1) \times 10^6\ \mathrm{M}^{-1}$ observed for pH 7.0.

3.2. Effect of BSA upon QD Interaction with TMPyP Porphyrin

Due to the presence of four positive side groups in its structure TMPyP porphyrin possesses 4+ charge in the pH range from 2.0 up to 9.0. These series of experiments were made at pH 4.0 and pH 7.0. However, the results, obtained for these two pHs were quite similar. Therefore, we present here only the results obtained in aqueous phosphate buffer solution at pH 7.0.

Interaction between CdTe-3MPA QD and TMPyP porphyrin in water solutions is characterized by formation of a charge transfer complex between negatively charged MPA groups of QD and positively charged methyl-pyridinium groups of TMPyP [28]. The complex is characterized by optical absorption peaks at 455 nm, 585 nm and 629 nm and a fluorescence peak at 632 nm (Figure 3). The fluorescence decay curve is monoexponential with the lifetime $\tau_{\mathrm{TMPyP\_QD}}$= (5.3 ± 0.2) ns (Figure 3, inset).

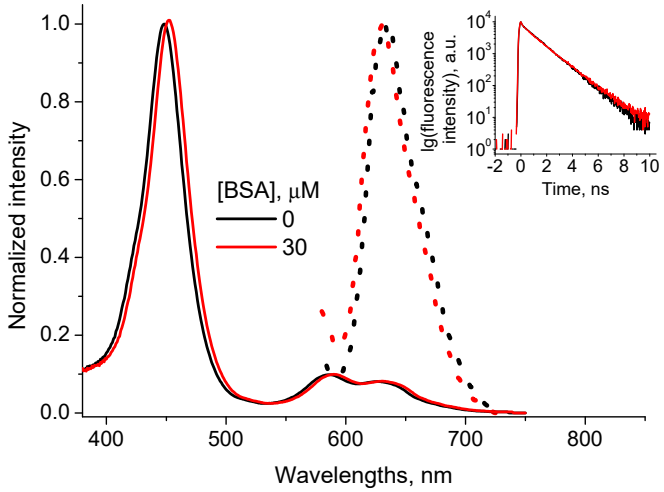

Figure 3. Normalized optical absorption (solid lines) and fluorescence (points) spectra (λ_{ex} = 455 nm) of the CdTe-3MPA … TMPyP complex in the presence of 0 and 30 μM BSA (inset: the complex fluorescence decay curves, λ_{ex} = 455 nm, λ_{em} = 650 nm).

The binding constant, determined from TMPyP fluorescence quenching by QD was $K_{TMPyP\_QD} = (6.0 \pm 0.5) \times 10^6$ M^{-1} [28].

The addition of BSA to the solution with formed CdTe-3MPA … TMPyP complex induces changes neither in the complex absorption and fluorescence spectra nor in the profile of the fluorescence decay curve (Figure 3).

Another series of experiments was made adding QD into the solution containing TMPyP and BSA. It was shown formerly [37] that TMPyP and BSA form a complex characterized by the optical absorption spectrum with Soret peak at 425 nm and three peaks in the Q region (Figure 4A) and fluorescence spectrum with a peak at 629 nm (Figure 4B). The binding constant of TMPyP with BSA was estimated as $K_{TMPyP\_BSA} = 7.3 \times 10^5$ M^{-1} [37].

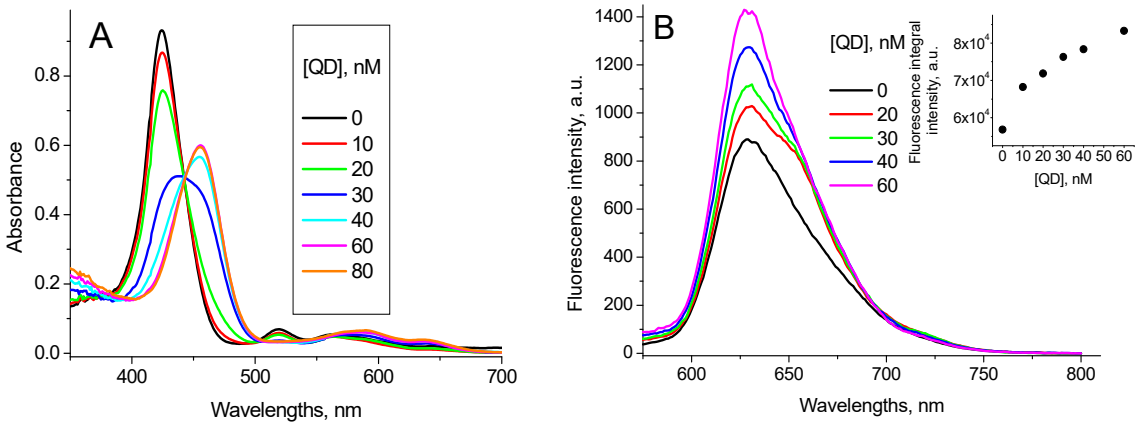

Figure 4. Absorption (**A**) and fluorescence (**B**) spectra (λ_{ex} = 445 nm) of 5 μM TMPyP solution in the presence of 30 μM BSA at different CdTe-3MPA QD concentrations. (The fluorescence spectra were recalculated subtracting the respective QD emission from the experimental ones).

The addition of QD into the TMPyP + BSA solution induces the reduction of the absorption peak at 425 nm and formation of a new absorption peak at 455 nm. This new absorption peak coincides with that of CdTe-3MPA … TMPyP complex (see Figure 3). Besides, the QD addition induces increase of the solution fluorescence intensity. Thus, we can associate these spectral changes with the formation of CdTe-3MPA … TMPyP charge transfer complex even in the BSA presence.

Binding constant of TMPyP with QD in the presence of BSA was calculated from the dependence of the integral fluorescence on the QD concentration using the Equation (7), which led to $K_{TMPyP\_QD + BSA} = (10 \pm 3) \times 10^6$ M^{-1}, close to that obtained in the BSA absence.

Thus, we can affirm that BSA in the solution does not destruct CdTe-3MPA ... TMPyP complex already formed, and does not reduce the probability of its formation, as well. This could be explained by the fact that the constant of the CdTe-3MPA ... TMPyP complex formation is approximately 10 times larger than that for TMPyP binding with BSA and 5 time larger than for CdTe-3MPA binding with BSA. Therefore, in the system of equilibria

$$\text{CdTe-3MPA} + \text{TMPyP} \Leftrightarrow \text{CdTe-3MPA} \ldots \text{TMPyP} \quad K_{TMPyP\_QD} = (6.0 \pm 0.5) \times 10^6 \text{ M}^{-1}$$

$$\text{BSA} + \text{TMPyP} \Leftrightarrow \text{BSA} \ldots \text{TMPyP} \quad K_{TMPyP\_BSA} = 7.3 \times 10^5 \text{ M}^{-1}$$

$$\text{CdTe-3MPA} + \text{BSA} \Leftrightarrow \text{CdTe-3MPA} \ldots \text{BSA} \quad K_{QD\_BSA} = (1.2 \pm 0.1) \times 10^6 \text{ M}^{-1}$$

the first one should be predominant.

Taking into account that IP of BSA is at pH 4.7, at pH 7.0 its net charge is negative and the electrostatic attraction should stimulate its binding with positively charged TMPyP molecules. However, TMPyP interaction with CdTe-3MPA QD appears stronger. This may be due to stabilization of TMPyP-QD contact via charge transfer complex formation.

The question is whether the CdTe-3MPA ... TMPyP complex can bind with BSA. However, no spectral changes have been observed which could be associated with the formation of this complex.

3.3. Effect of BSA on Interaction of QD with TPPS$_4$ Porphyrin

Due to the presence of four nitrogen atoms in the porphyrin ring structure $TPPS_4$ porphyrin can be biprotonated, with the pK_a point close to pH 5.0 [38]. Therefore, at pH 7.0, where $TPPS_4$ is in the non-protonated form, it possesses a charge 4^-, while at pH 4.0, where it is in the biprotonated form, its charge is 2^-. This determines the difference in the $TPPS_4$ behavior at these two pHs. Therefore, at pH 7.0 the non-protonated $TPPS_4$ is characterized by the optical absorption spectrum with Soret peak at 413 nm and four peaks in the Q-region, the largest localized at 518 nm, and fluorescence with maximum at 640 nm (Figure 5) and the lifetime $\tau_{pH7} = 8.5$ ns. Biprotonated $TPPS_4$ possesses the absorption spectrum with Soret peak at 434 nm and three peaks in the Q-region with the largest one at 646 nm and fluorescence with maximum at 665 nm (Figure 5) and the fluorescence lifetime of $\tau_{pH4} = 3.6$ ns [39].

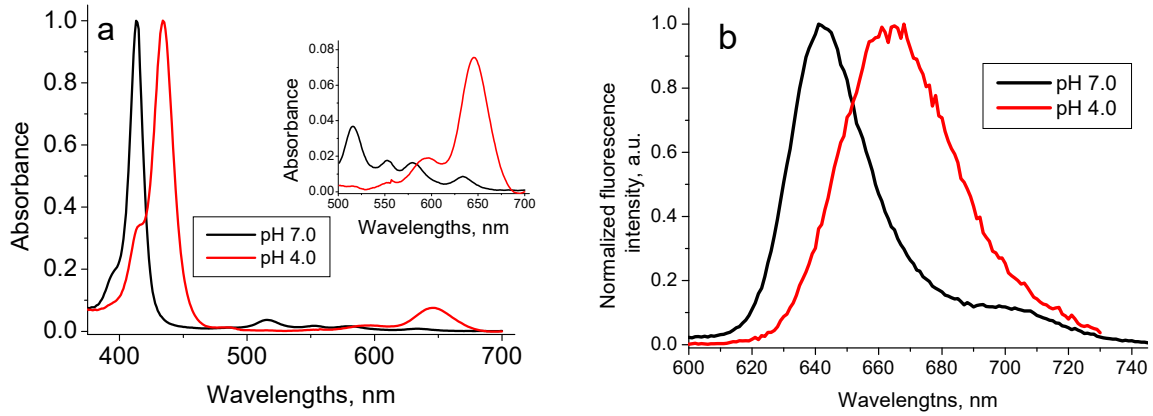

Figure 5. Normalized optical absorption (**a**) and fluorescence spectra ($\lambda_{ex} = 420$ nm) (**b**) of 1.6 μM $TPPS_4$ in the bi-protonated (pH 4.0) and non-protonated (pH 7.0) states [39].

3.3.1. Effect of BSA on Interaction of QD with $TPPS_4$ Porphyrin at pH 7.0

Recently we have demonstrated [29] that at pH 7.0 interaction of $TPPS_4$ with CdTe-3-MPA QD is realized via energy transfer from QD to $TPPS_4$. This interaction induces no changes in absorption and emission spectra of both $TPPS_4$ and QD; however, it reduces the QD luminescence intensity. The binding constant of the non-protonated $TPPS_4$ with QD was estimated as $K_{TPPS\_QD\ pH7} = (2.5 \pm 0.1) \times 10^6\ M^{-1}$ [29].

Interaction of $TPPS_4$ with BSA has recently been studied in [37]. Addition of BSA into the $TPPS_4$ solutions at pH 7.0 induces the shift of the $TPPS_4$ Soret absorption band from λ = 412 nm to λ = 422 nm and the fluorescence peak from λ = 645 nm to λ = 654 nm. The $TPPS_4$ fluorescence intensity increases (Figure 6), and lifetime is practically unchanged $\tau_{TPPS\_BSA\ pH7} = (10.8 \pm 0.1)$ ns. The $TPPS_4$-BSA binding constant is $K_{TPPS\_BSA\ pH7} = 3.2 \times 10^6\ M^{-1}$ [37].

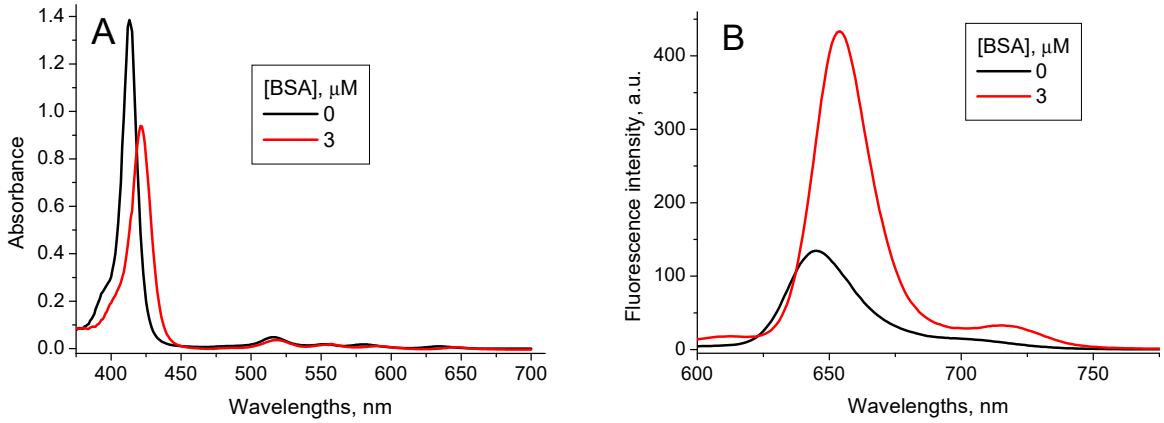

Figure 6. Optical absorption (**A**) and fluorescence (λ_{ex} = 417 nm) (**B**) spectra of 1.6 μM $TPPS_4$ water solution at pH 7.0 in the absence and presence of 3 μM BSA [37].

The addition of BSA into the $TPPS_4$ … QD solution shifts the $TPPS_4$ absorption band from 412 nm to 422 nm and a new band centered at 436 nm appears. Simultaneously, the $TPPS_4$ … QD complex emission increases and an emission peak at 650 nm is formed (Figure 7).

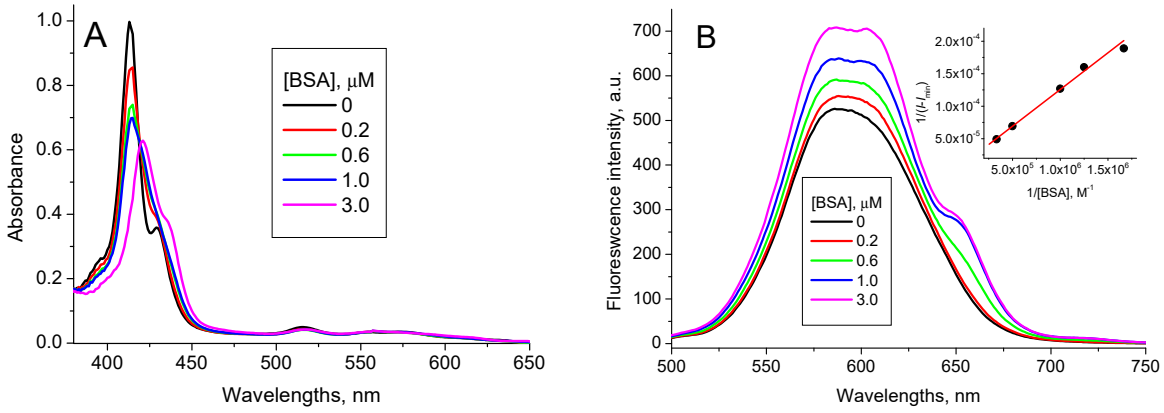

Figure 7. 1.6 μM $TPPS_4$ optical absorption (**A**) and fluorescence spectra (λ_{ex} = 420 nm) (**B**) in the presence of 400 nM CdTe-MPA QD at different BSA concentrations (pH 7.0), (inset: the fitting of the fluorescence integral intensity in accordance with the Equation (7)).

These new peaks combine with no peak of either pure $TPPS_4$, pure CdTe-3-MPA QD or $TPPS_4$ … CdTe-3-MPA complex. Therefore, we believe they reflect formation of a new mixed $TPPS_4$ … CdTe-3-MPA … BSA complex. The binding constant calculated from the fluorescence data in accordance with the Equation (7) is $K_{TPPS\_QD\ +\ BSA\ pH7} = (6.5 \pm 0.2) \times 10^6\ M^{-1}$.

Addition of QD into the $TPPS_4$ + BSA mixed solution induces no changes in the absorption and fluorescence spectra of these solutions, demonstrating that binding of $TPPS_4$ with BSA at pH 7.0 prevents the formation of $TPPS_4$ ... CdTe-3-MPA complex and consequently the formation of the mixed $TPPS_4$ ... CdTe-3-MPA ... BSA complex.

Effective binding of negatively charged non-protonated $TPPS_4$ with BSA, which at pH 7.0 is also negatively charged, shows that in this case electrostatic repulsion is not dominant and other types of interaction, such as a hydrophobic one, should be responsible for porphyrin binding with BSA. High stability of the $TPPS_4$ ... CdTe-3-MPA complex cannot be associated with the electrostatic interaction, as well, since at pH 7.0 the MPA groups of QD are non-protonated and do not possess a positive charge. The effective contribution of non-electrostatic interactions in the non-protonated $TPPS_4$ + QD + BSA system follows from the fact of formation of the mixed $TPPS_4$ ... QD ... BSA complex. However, more detailed and justified conclusions about the nature and contributions of various types of interaction in this complex system require more profound studies using other experimental techniques besides spectroscopic ones.

3.3.2. Effect of BSA on Interaction of QD with $TPPS_4$ Porphyrin at pH 4.0

As it has been demonstrated earlier [29], at pH 4.0 interaction of $TPPS_4$ with CdTe-3-MPA QD occurs via two mechanisms: the proton transfer from $TPPS_4$ to QD and the energy transfer from QD to $TPPS_4$, the first one being predominant. The proton transfer changes the $TPPS_4$ absorption and fluorescence spectra, characteristic for the biprotonated $TPPS_4$, to those of the non-protonated form (Figure 8). The fluorescence lifetime changes from $\tau_{TPPS\ pH4} = (3.6 \pm 0.2)$ ns to $\tau_{TPPS\_BSA\ pH4} = (8.5 \pm 1)$ ns, which is also characteristic for the non-protonated $TPPS_4$.

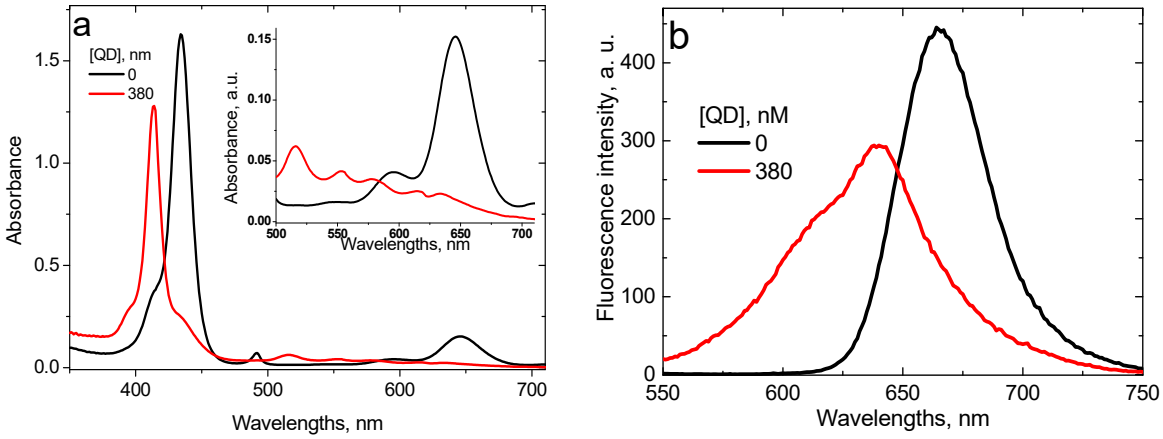

Figure 8. Optical absorption (**a**) and fluorescence (**b**) (λ_{ex} = 420 nm) spectra of the 1.6 μM $TPPS_4$ solution at pH 4.0 in the absence and in the presence of 380 nM CdTe-3-MPA QD [29].

The binding constant of $TPPS_4$ with CdTe-3-MPA QD, calculated from fluorescence data is $K_{TPPS\_QDpH4} = (2.4 \pm 0.2) \times 10^6\ M^{-1}$ [29].

Addition of BSA into the $TPPS_4$ solutions at pH 4.0 induces the $TPPS_4$ deprotonation, as well, leading to spectral characteristics equal to those of the non-protonated $TPPS_4$ bound with BSA: Soret peak at λ = 422 nm, fluorescence peak at 654 nm and fluorescence lifetime τ = 10.8 ns. The obtained binding constant of $TPPS_4$ with BSA is $K_{TPPS\_BSA\ pH4} = 1.5 \times 10^8\ M^{-1}$ [37].

Addition of BSA into the $TPPS_4$ ... CdTe-3-MPA complex solution changes the profile and peak positions of the optical absorption and fluorescence spectra in such a way that the final ones coincide with those of $TPPS_4$ bound with BSA (Figure 9). The fluorescence intensity and lifetime increase (Figure 9, inset), which is also characteristic for $TPPS_4$ binding with BSA. This could mean that addition of BSA destructs the $TPPS_4$ ... CdTe-3-MPA complex in favor of the $TPPS_4$ complex with BSA. At the same time, the

calculation of the $TPPS_4$ binding constant with BSA using the Equation (3) leads to $K_{TPPS_{QD}+BSApH4} = (1.2 \pm 0.2) \times 10^{10}$ M^{-1} (Figure 10). This value is ≈100 times larger than that for $TPPS_4$ binding with BSA in the absence of CdTe-3-MPA QD. This demonstrates that the $TPPS_4$ binding with QD increases the probability of its binding with BSA.

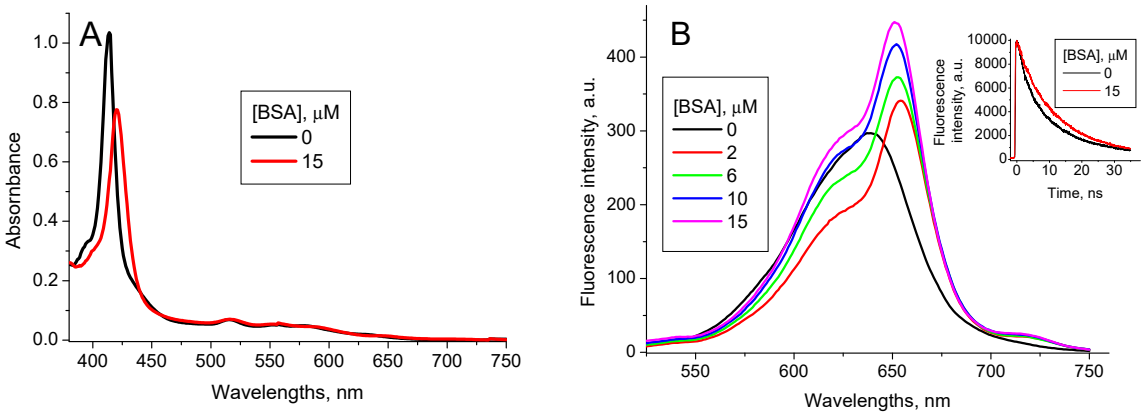

Figure 9. $TPPS_4$ optical absorption (**A**) and fluorescence (**B**) spectra (λ_{ex} = 417 nm) at pH 4.0 in the presence of 380 nM CdTe-3-MPA QD for different BSA concentrations (Inset: the fluorescence decay curves in the absence and presence of 15 μM BSA, λ_{ex} = 420 nm, λ_{em} = 650 nm).

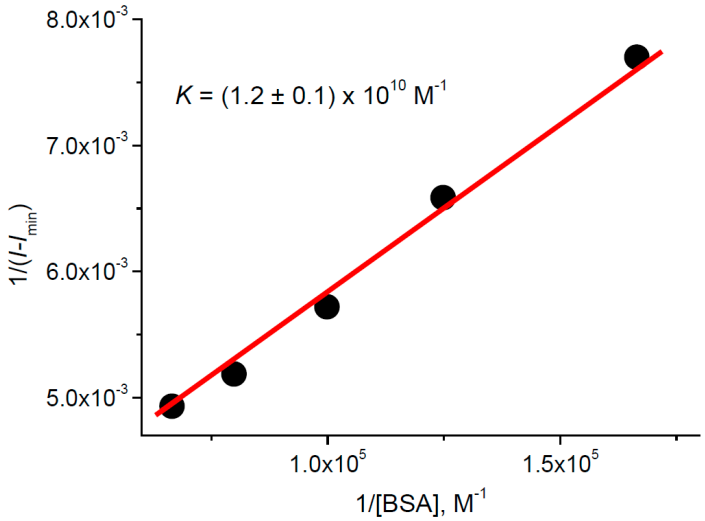

Figure 10. Fitting in accordance with the Equation (3) of the $TPPS_4$ fluorescence intensity in the presence of 380 nM CdTe-3-MPAQD in function of BSA concentration at pH 4.0.

When QD is added into the $TPPS_4$ + BSA solutions, no changes either in its optical absorption and fluorescence spectra or in the fluorescence lifetime occur, which demonstrates that the porphyrin binding with BSA blocks its binding with QD.

4. Conclusions

Depending on the porphyrin characteristics, principally its charge state, its interaction with bovine serum albumin (BSA) manifests in different forms.

In the case of *meso*-tetra methyl pyridyl porphyrin (TMPyP), which possesses charge 4+ and forms a charge transfer complex with CdTe-3-MPA quantum dots, albumin neither destructs this complex already formed nor reduces the probability of its formation.

For *meso*-tetrakis(p-sulfonato-phenyl) porphyrin ($TPPS_4$), non-protonated at pH 7.0, which has a charge 4− and forms an energy transfer complex with CdTe-3-MPA quantum dots, BSA is able to form a mixed $TPPS_4$ ... CdTe-3-MPA ... BSA complex.

In the case of the biprotonated $TPPS_4$ with charge 2− at pH 4.0, for which the complexation with CdTe-3-MPA includes both an energy transfer and a proton transfer, BSA destructs this complex in favor of the $TPPS_4$ ... BSA one and prevents $TPPS_4$ from complexation with QD. Moreover, surprisingly, $TPPS_4$ complexation with QD increases the probability of its binding with BSA.

We consider this study as the first step in investigation of effects of albumins upon the porphyrin complexation with quantum dots. To clarify the mechanisms of these effects, more detailed studies are necessary with the help of various experimental techniques, besides the spectroscopic ones. However, since the main purpose of this study is to evaluate the perspective of application of porphyrin ... quantum dot complexes in photochemotherapy, which is based on light exposure, the spectroscopic results presented in this paper can be important for application of porphyrin ... quantum dot complexes in medicine for fluorescence diagnostics and photodynamic therapy.

Author Contributions: A.L.S.P.: realizing experiments, data analysis, discussions and text preparation; L.N.C.M.: compound synthesis, discussions, text evaluation; R.S.d.S.: discussions, text evaluation; I.E.B.: conceptualization, realizing experiments, data analysis, discussions and text preparation. All authors have read and agreed to the published version of the manuscript.

Funding: The authors are indebted to CNPq (Grant No. 405389/2018-3, 306243/2018-0, 304863/2017-3 and 405389/2018-3) and FAPESP (Grant No. 2016/12707-0, 2019/19448-8) Brazilian agencies for partial financial support. The pos-graduate student André L. S. Pavanelli receives his Doctorship support from Coordenação de Aperfeiçoamento de Pessoal de Nível Superior -Brasil (CAPES)-Finance Code 001.

Data Availability Statement: All original data related in this study are presented in the manuscript text and in cited articles.

Conflicts of Interest: The authors declare no conflict of interest.

References

1. Xue, X.; Lindstrom, A.; Li, Y. Porphyrin-Based Nanomedicines for Cancer Treatment. *Bioconj. Chem.* **2019**, *30*, 1585–1603. [CrossRef]
2. Gomes, A.T.P.C.; Neves, M.G.P.M.S.; Cavaleiro, J.A.S. Cancer, Photodynamic Therapy and Porphyrin-Type Derivatives. *An. Acad. Bras. Ciênc.* **2018**, *90* (Suppl. 2). [CrossRef]
3. Kou, J.; Dou, D.; Yang, L. Porphyrin photosensitizers in photodynamic therapy and its applications. *Oncotarget.* **2017**, *8*, 81591–81603. [CrossRef]
4. Cui, L.; Chen, J.; Zheng, G. Chapter 7: Porphyrin Nanoparticles for Cancer Imaging and Phototherapy. In *Handbook of Photodynamic Therapy*, 1st ed.; World Scientific Publishing Company: Singapore, 2016; pp. 273–293. [CrossRef]
5. Pushpan, S.K.; Venkatraman, S.; Anand, V.G.; Sankar, J.; Parmeswaran, D.; Ganesan, S.; Chandrashekar, T.K. Porphyrins in Photodynamic Therapy—A Search for Ideal Photosensitizers. *Anti-Curr. Med. Chem.—Anti-Cancer Agents* **2002**, *2*, 187–207. [CrossRef]
6. Shi, J.; Liu, T.W.B.; Chen, J.; Green, D.; Jaffray, D.; Wilson, B.C.; Wang, F.; Zheng, G. Transforming a Targeted Porphyrin Theranostic Agent into a PET Imaging Probe for Cancer. *Theranostics* **2011**, *1*, 363–370. [CrossRef] [PubMed]
7. Ricchelli, F.; Gobbo, S. Porphyrins as fluorescent probes for monitoring phase transitions of lipid domains in biological membranes. Factors influencing the microenvironment of haematoporphyrin and protoporphyrin in liposomes. *J. Photochem. Photobiol. B Biol.* **1995**, *29*, 65–70. [CrossRef]
8. Liu, F.; Shen, Y.-C.; Chen, S.; Yan, G.-P.; Zhang, Q.; Guo, Q.-Z.; Gu, Y.-T. Tumor-Targeting Fluorescent Probe Based on Naphthalimide and Porphyrin Groups. *Biol. Chem. Chem. Biol.* **2020**, *5*, 7680–7684. [CrossRef]
9. Burda, C.; Chen, X.; Narayanan, R.; El-Sayed, M.A. Chemistry and Properties of Nanocrystals of Different Shapes. *Chem. Rev.* **2005**, *105*, 1025–1102. [CrossRef] [PubMed]
10. Buhbut, S.; Itzhakov, S.; Tauber, E.; Shalom, M.; Hod, I.; Geiger, T.; Garini, Y.; Oron, D.; Zaban, A. Built-in Quantum Dot Antennas in Dye-Sensitized Solar Cells. *ACS Nano* **2010**, *4*, 1293–1298. [CrossRef]
11. Mokhlespour, S.; Haverkort, J.E.M.; Slepyan, G.Y.; Maksimenko, S.A.; Hoffmann, A. Quantum Dot Lattice as Nano-Antenna for Collective Spontaneous Emission. In *Fundamental and Applied Nano-Electromagnetics*; Maffucci, A., Maksimenko, S.A., Eds.; NATO Science for Peace and Security Series B: Physics and Biophysics; Springer: Dordrecht, The Netherlands, 2016. [CrossRef]
12. Nabiev, I.; Rakovich, A.; Sukhanova, A.; Lukashev, E.; Zagidullin, V.; Pachenko, V.; Rakovich, Y.P.; Donegan, J.F.; Rubin, A.B.; Govorov, A.O. Fluorescent Quantum Dots as Artificial Antennas for Enhanced Light Harvesting and Energy Transfer to Photosynthetic Reaction Centers. *Angew. Chem. Int. Ed. Engl.* **2010**, *49*, 7217–7221. [CrossRef] [PubMed]

13. Borissevitch, I.E.; Lukashev, E.P.; Oleinikov, I.P.; Pavanelli, A.L.S.; Gonçalves, P.J.; Knox, P.P. Electrostatic interactions and covalent binding effects on the energy transfer between quantum dots and reaction centers of purple bacteria. *J. Lumin.* **2019**, *207*, 129–136. [CrossRef]
14. Zhang, Y. Surface Functionalization of Quantum Dots for Biotechnological Applications. Ph.D. Thesis, Iowa State University, Ames, IA, USA, April 2012.
15. Karakoti, A.S.; Shukla, R.; Shanker, R.; Singh, S. Surface functionalization of quantum dots for biological applications. *Adv. Colloid Interface Sci.* **2015**, *215*, 28–45. [CrossRef]
16. Chandan, R.H.; Schiffman, J.D.; Balakrishna, R.G. Quantum dots as fluorescent probes: Synthesis, surface chemistry, energy transfer mechanisms, and applications. *Sens. Actuators B Chem.* **2018**, *258*, 1191–1214. [CrossRef]
17. Rizvi, S.B.; Ghaderi, S.; Keshtgar, M.; Seifalian, A.M. Semiconductor quantum dots as fluorescent probes for in vitro and in vivo bio-molecular and cellular imaging. *Nano Rev.* **2010**, *1*. [CrossRef] [PubMed]
18. Frasco, M.F.; Chaniotakis, N. Bioconjugated quantum dots as fluorescent probes for bioanalytical applications. *Anal. Bioanal Chem.* **2010**, *396*, 229–240. [CrossRef]
19. Samia, A.C.S.; Dayal, S.; Burda, C. Quantum Dot-based Energy Transfer: Perspectives and Potential for Applications in Photodynamic Therapy. *Photochem. Photobiol.* **2006**, *82*, 617–625. [CrossRef]
20. Martynenko, I.V.; Kuznetsova, V.A.; Orlova, A.O.; Kanaev, P.A.; Maslov, V.G.; Loudon, A.; Zaharov, V.; Parfenov, P.; Gun'ko, Y.K.; Baranov, A.V. Chlorin e6–ZnSe/ZnS quantum dots based system as reagent for photodynamic therapy. *Nanotechnology* **2015**, *26*, 055102. [CrossRef] [PubMed]
21. Dayal, S.; Krolicki, R.; Lou, Y.; Qiu, X.; Berlin, J.C.; Kenney, M.E.; Burda, C. Femtosecond time-resolved energy transfer from CdSe nanoparticles to phthalocyanines. *Appl. Phys. B Lasers Opt.* **2006**, *84*, 309–315. [CrossRef]
22. Gromova, Y.A.; Orlova, A.O.; Maslov, V.G.; Fedorov, A.V.; Baranov, A.V. Fluorescence energy transfer in quantum dot/azo dye complexes in polymer track membranes. *Nanoscale Res. Lett.* **2013**, *8*, 452. [CrossRef] [PubMed]
23. Białek, R.; Burdziński, G.; Gibasiewicz, K.; Worch, R.; Grzyb, J. Competition between Photoinduced Electron Transfer and Resonance Energy Transfer in an Example of Substituted Cytochrome c–Quantum Dot Systems. *J. Phys. Chem. B* **2021**, *125*, 3307–3320. [CrossRef]
24. Jhonsi, A.M.; Renganathan, R. Investigations on the photoinduced interaction of water soluble thioglycolic acid (TGA) capped CdTe quantum dots with certain porphyrins. *J. Colloid Interface Sci.* **2010**, *344*, 596–602. [CrossRef]
25. Zhang, X.; Liu, Z.; Ma, L.; Hossu, M.; Chen, W. Interaction of porphyrins with CdTe quantum dots. *Nanotechnology* **2011**, *22*, 195501–195510. [CrossRef] [PubMed]
26. Borissevitch, I.E.; Parra, G.; Zagidullin, V.; Lukashev, E.; Knox, P.; Pashenko, V.; Rubin, A. Cooperative effects in CdSe/ZnS-PEGOH quantum dot luminescence quenching by a water soluble porphyrin. *J. Lumin.* **2013**, *134*, 83–87. [CrossRef]
27. Parra, G.G.; Ferreira, L.P.; Gonçalves, P.J.; Sizova, S.V.; Oleinikov, V.A.; Morozov, V.N.; Kuzmin, V.A.; Borissevitch, I.E. Stimulation of Cysteine-Coated CdSe/ZnS Quantum Dot Luminescence by *meso*-Tetrakis (p-sulfonato-phenyl) Porphyrin. *Nanoscale Res. Lett.* **2018**, *13*. [CrossRef]
28. Parra, G.G.; Pavanelli, A.L.S.; Franco, L.P.; Máximo, L.N.C.; da Silva, R.S.; Borissevitch, I. Interaction of CdTe-MPA quantum dots with meso-tetra methyl pyridyl porphyrin. Charge transfer complex formation. *J. Photochem. Photobiol. A Chem.* **2020**, *398*, 112580. [CrossRef]
29. Pavanelli, A.L.S.; Máximo, L.N.C.; da Silva, R.S.; Borissevitch, I. Interaction between $TPPS_4$ porphyrin and CdTe-3-MPA quantum dot: Proton and energy transfer. *J. Lumin.* **2021**, *237*, 118213. [CrossRef]
30. Peters, T., Jr. All about Albumin. In *Biochemistry, Genetics, and Medical Applications*; Academic Press: Cambridge, MA, USA, 1996; ISBN 9780080527048.
31. Kratz, F.; Beyer, U. Serum proteins as drug carriers of anticancer agents, a review. *Drug Deliv.* **1998**, *5*, 281–299. [CrossRef]
32. Dennis, M.S.; Jin, H.; Dugger, D.; Yang, R.; McFarland, L.; Ogasawara, A.; Williams, S.; Cole, M.J.; Ross, S.; Schwall, R. Imaging Tumors with an Albumin-Binding Fab, a Novel Tumor-Targeting Agent. *Cancer Res.* **2007**, *67*, 254–261. [CrossRef]
33. Franco, L.P.; Cicillini, S.; Biazzotto, J.; Schiavon, M.; Mikhailovsky, A.; Burks, P.; Garcia, J.; Ford, P.; Silva, R. Photoreactivity of a quantum dot-ruthenium nitrosyl conjugate. *J. Phys. Chem. A* **2014**, *118*, 12184–12191. [CrossRef]
34. Yu, W.W.; Qu, L.; Guo, W.; Peng, X. Experimental Determination of the Extinction Coefficient of CdTe, CdSe, and CdS Nanocrystals. *Chem. Mater.* **2003**, *15*, 2854–2860. [CrossRef]
35. Tabak, M.; Borisevitch, I.E. Interaction of dipyridamole with micelles of lysophosphatidylcholine and with bovine serum albumin: Fluorescence studies. *BBA—Gen. Sub.* **1992**, *1116*, 241–249. [CrossRef]
36. Patty, F.A. (Ed.) *Industrial Hygiene and Toxicology*, 2nd ed.; John Wiley & Sons, Inc.: New York, NY, USA, 1963; Volume II. [CrossRef]
37. Borissevitch, I.E.; Tominaga, T.T.; Imasato, H.; Tabak, M. Fluorescence and optical absorption study of interaction of two water soluble porphyrins with bovine serum albumin. The role of albumin and porphyrin aggregation. *J. Lumin.* **1996**, *69*, 65–76. [CrossRef]
38. Aggarwal, L.P.F.; Borissevitch, I.E. On the dynamics of the TPPS4 aggregation in aqueous solutions: Successive formation of H and J aggregates. *Spectrochim. Acta A Mol. Biomol. Spectrosc.* **2006**, *63*, 227–233. [CrossRef] [PubMed]
39. Gonçalves, P.J.; De Boni, L.; Barbosa Neto, N.M.; Rodrigues, J.J.; Zílio, S.C.; Borissevitch, I.E. Effect of protonation on the photophysical properties of meso-tetra(sulfonatophenyl) porphyrin. *Chem. Phys. Lett.* **2005**, *407*, 236–241. [CrossRef]